

## Electronic supplementary information

### Europium shuttle for launching perovskites to space: using Eu<sup>2+</sup>/Eu<sup>3+</sup> redox chemistry to boost photostability and radiation hardness of complex lead halides

Marina I. Ustinova<sup>1</sup>, Lyubov A. Frolova<sup>1\*</sup>, Alexandra V. Rasmetyeva<sup>2</sup>, Nikita A. Emelianov<sup>1</sup>, Maxim N. Sarychev<sup>2</sup>, Gennadii V. Shilov<sup>1</sup>, Pavel P. Kushch<sup>1</sup>, Nadezhda N. Dremova<sup>1</sup>, Galina A. Kichigina<sup>1</sup>, Andrey I. Kukharenko<sup>2,3</sup>, Dmitry P. Kiryukhin,<sup>1</sup> Ernst Z. Kurmaev<sup>2,3</sup>, Ivan S. Zhidkov<sup>2,3\*</sup> and Pavel A. Troshin<sup>4,1\*</sup>

<sup>1</sup> Federal Research Center for Problems of Chemical Physics and Medicinal Chemistry of the Russian Academy of Sciences, Academician Semenov ave. 1, 142432 Chernogolovka, Russia

<sup>2</sup> Institute of Physics and Technology, Ural Federal University, Mira 19 Street, Yekaterinburg 620002, Russia

<sup>3</sup> M. N. Mikheev Institute of Metal Physics of Ural Branch of Russian Academy of Sciences, S. Kovalevskoi 18 Street, Yekaterinburg 620108, Russia

<sup>4</sup> Zhengzhou Research Institute of HIT, Longyuan East 7th 26, Jinshui District, Zhengzhou 450003, China

#### Contents

Figure S1. XRD patterns of MAPb<sub>1-x</sub>Eu<sub>x</sub>I<sub>3</sub> and Cs<sub>0.12</sub>FA<sub>0.88</sub>Pb<sub>1-x</sub>Eu<sub>x</sub>I<sub>3</sub> films with different Eu loadings;

Figure S2. The XRD pattern of the precipitate formed upon interaction of Eu<sup>2+</sup> with Pb<sup>2+</sup> in the presence of MAI and DMF solvent;

Figure S3. The XRD patterns of the PbI<sub>2</sub> films with and without Eu modification after 430 hours of exposure to light (85 mW/cm<sup>2</sup>, 32 °C);

Figure S4. AFM topography and IR s-SNOM images taken at the FA characteristic vibration frequency for Cs<sub>0.12</sub>FA<sub>0.88</sub>PbI<sub>3</sub> films after exposure to 1×10<sup>16</sup> e/cm<sup>2</sup> fluence of 8.5 MeV electrons;

Figure S5. The XPS analysis of the Cs<sub>0.12</sub>FA<sub>0.88</sub>PbI<sub>3</sub> and Cs<sub>0.12</sub>FA<sub>0.88</sub>Pb<sub>0.999</sub>Eu<sub>0.001</sub>I<sub>3</sub> films before and after the exposure of high-energy electrons;

Figure S6. The influence of Eu-loading on the photovoltaic characteristics of solar cells in the n-i-p structure;

Figure S7. The EQE spectra of the n-i-p solar cells;

Figure S8. Evolution of the EQE spectra of the p-i-n solar cells during receiving the different <sup>60</sup>Co  $\gamma$ -irradiation dose.

Table S1. Surface composition of the MAPb<sub>1-x</sub>Eu<sub>x</sub>I<sub>3</sub> perovskite films;

Table S2. Surface composition of the Cs<sub>0.12</sub>FA<sub>0.88</sub>Pb<sub>1-x</sub>Eu<sub>x</sub>I<sub>3</sub> perovskite films;

Table S3. The average and the best values of the photovoltaic characteristics of n-i-p devices;

Table S4. The average and the best values of the photovoltaic characteristics of solar cells in the p-i-n structure;

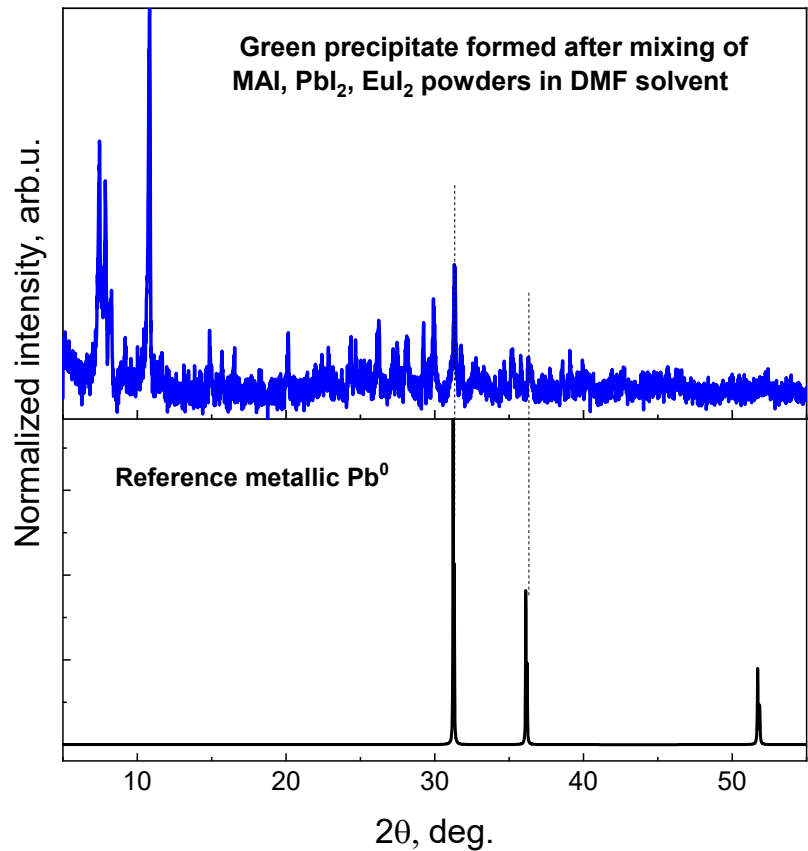


Figure S1. The XRD pattern of the precipitate formed upon interaction of Eu<sup>2+</sup> with Pb<sup>2+</sup> in the presence of MAI and DMF solvent.

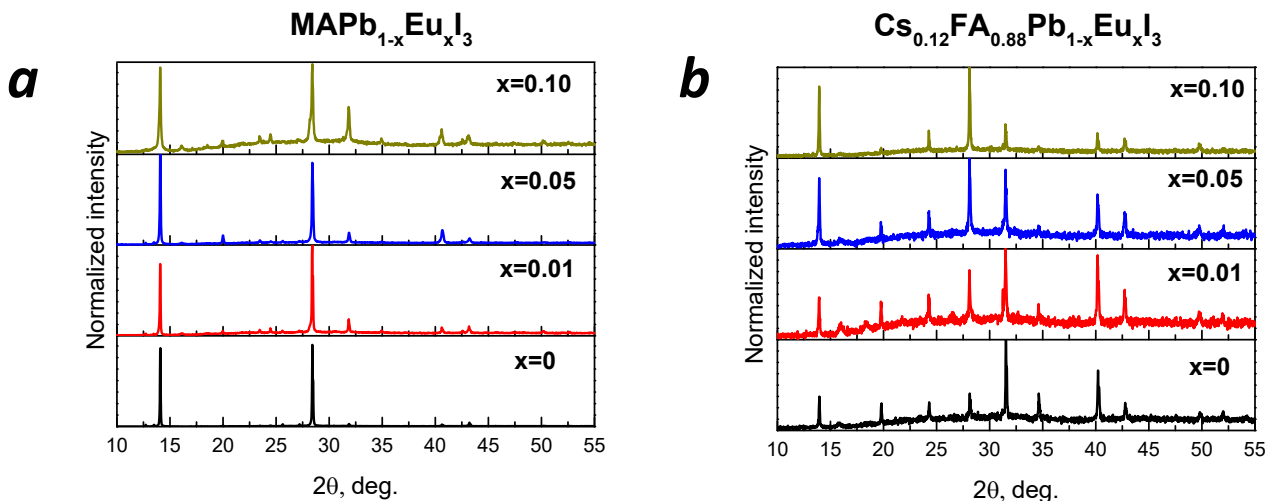


Figure S2. XRD patterns of MAPb<sub>1-x</sub>Eu<sub>x</sub>I<sub>3</sub> and Cs<sub>0.12</sub>FA<sub>0.88</sub>Pb<sub>1-x</sub>Eu<sub>x</sub>I<sub>3</sub> films with different Eu loadings.

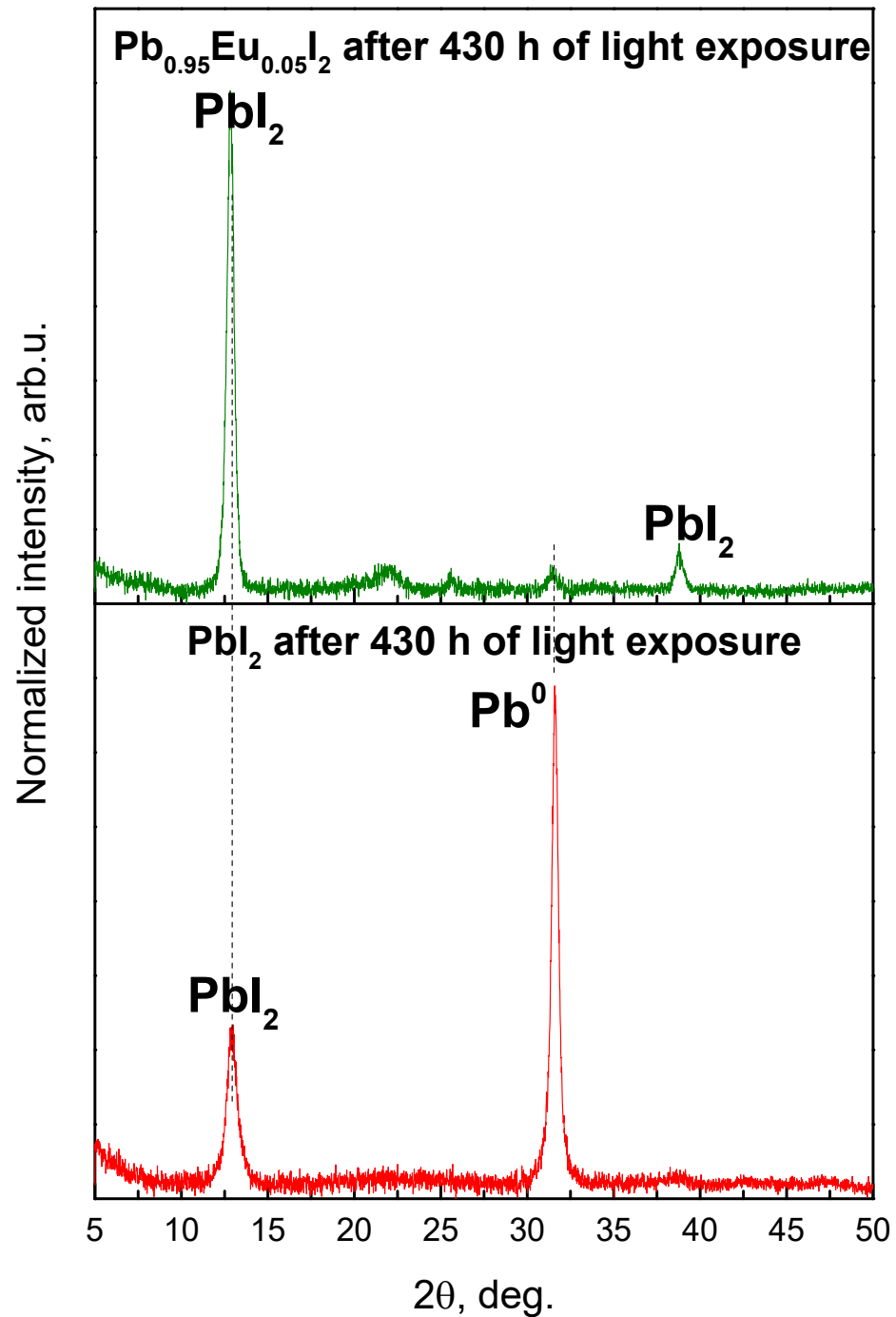


Figure S3. The XRD patterns of the  $\text{PbI}_2$  films with (top) and without (bottom) Eu modification after 430 hours of exposure to light ( $85 \text{ mW/cm}^2$ ,  $32^\circ\text{C}$ ).

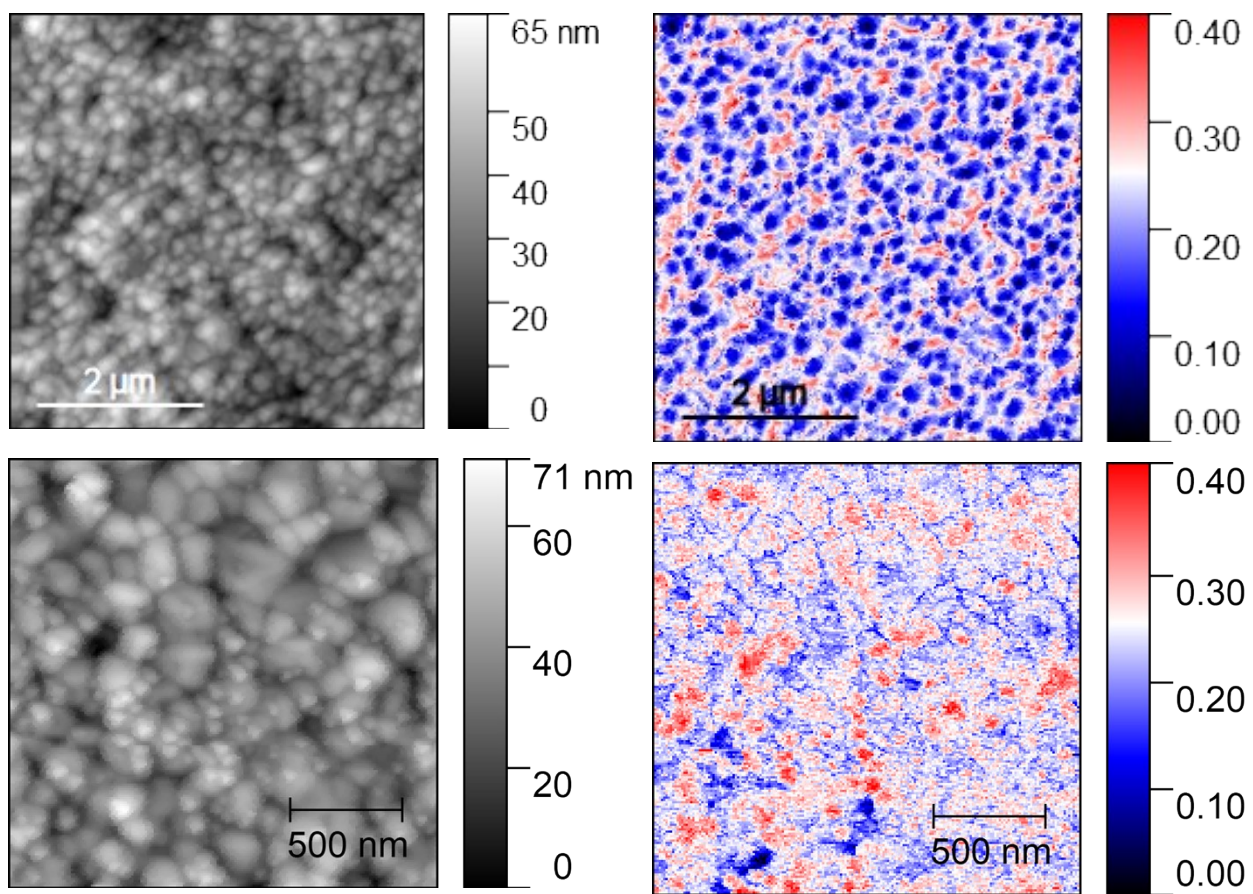


Figure S4. AFM topography (left column) and IR s-SNOM images taken at the FA characteristic vibration frequency for  $\text{Cs}_{0.12}\text{FA}_{0.88}\text{PbI}_3$  films after exposure to  $1 \times 10^{16} \text{ e/cm}^2$  fluence of 8.5 MeV electrons. The images are presented with  $5 \times 5 \mu\text{m}$  (top) and  $2 \times 2 \mu\text{m}$  (bottom) scalebars to show that the newly formed grains on the surface are enriched with FA cations.

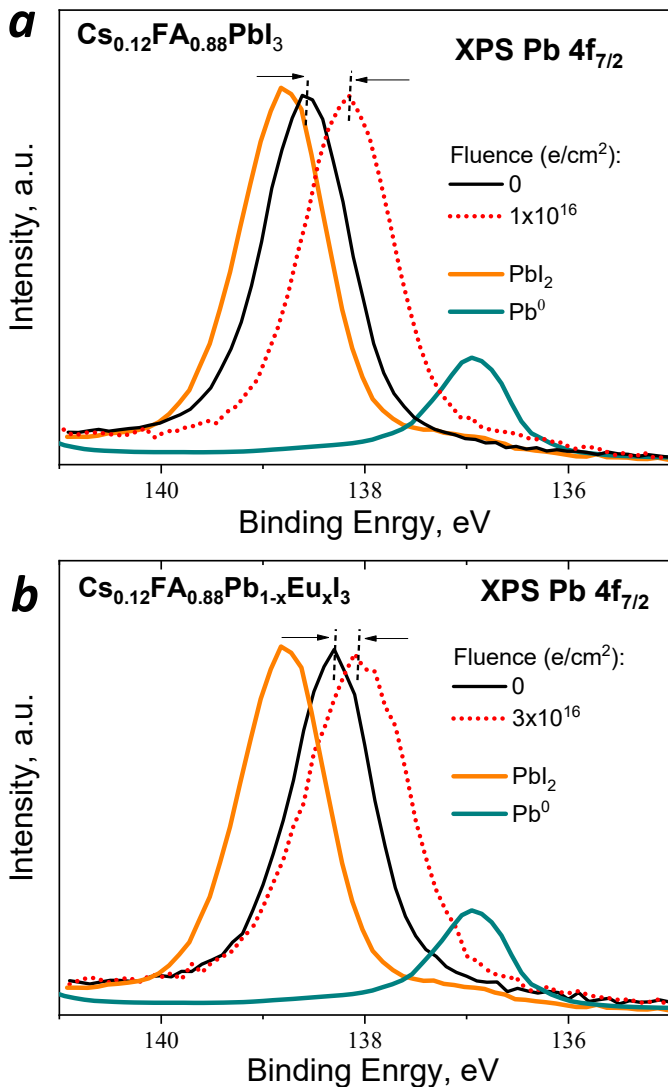
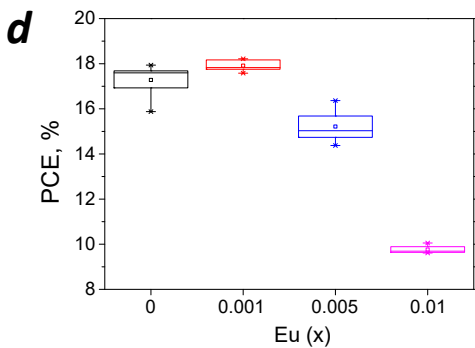
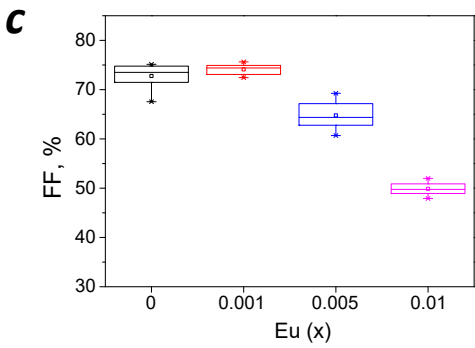
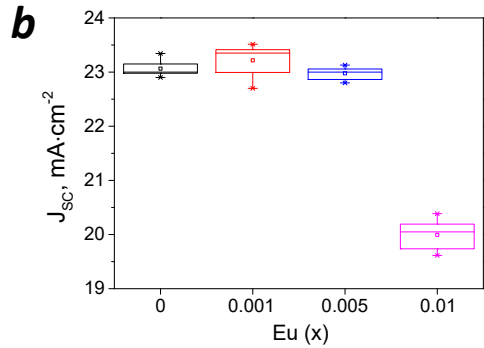
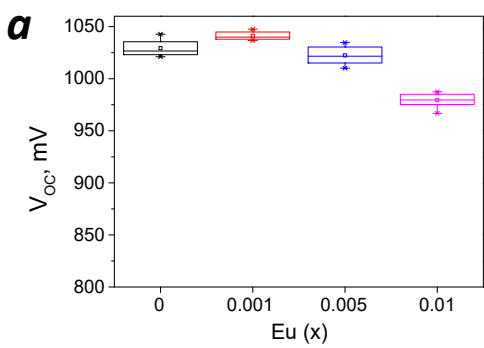


Figure S5. The XPS analysis of the Cs<sub>0.12</sub>FA<sub>0.88</sub>PbI<sub>3</sub> and Cs<sub>0.12</sub>FA<sub>0.88</sub>Pb<sub>0.999</sub>Eu<sub>0.001</sub>I<sub>3</sub> films before and after the exposure of high-energy electrons (1·10<sup>16</sup> and 3·10<sup>16</sup> e·cm<sup>-2</sup> doses, respectively).

### **MAPb<sub>1-x</sub>Eu<sub>x</sub>I<sub>3</sub>**



### **Cs<sub>0.12</sub>FA<sub>0.88</sub>Pb<sub>1-x</sub>Eu<sub>x</sub>I<sub>3</sub>**

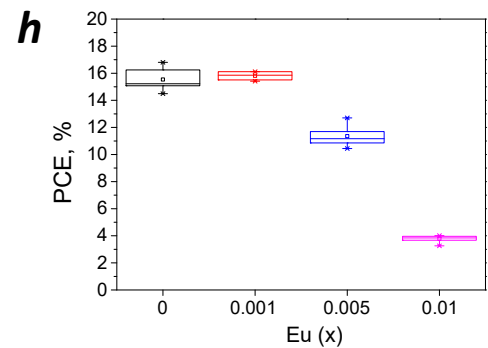
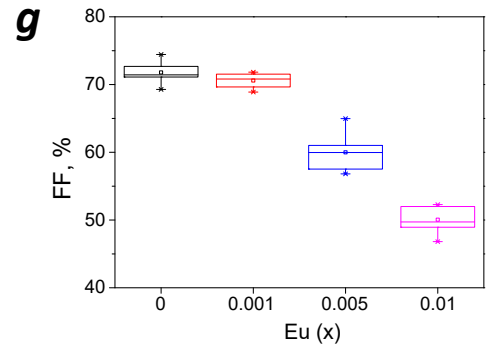
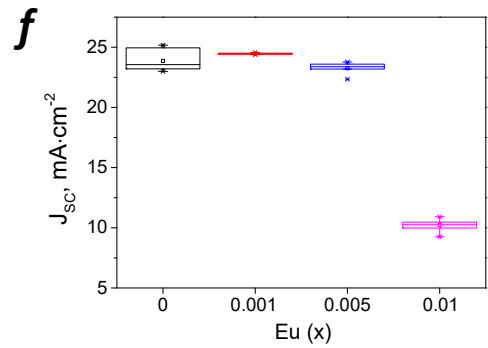
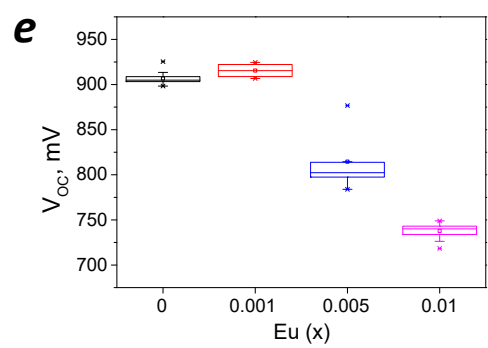


Figure S6. The influence of Eu-loading on the photovoltaic characteristics ( $V_{oc}$ ,  $J_{sc}$ , FF, and PCE) of n-i-p PSCs (ITO/SnO<sub>2</sub>/PCBA/Cs<sub>0.12</sub>FA<sub>0.88</sub>Pb<sub>1-x</sub>Eu<sub>x</sub>I<sub>3</sub> or MAPb<sub>1-x</sub>M<sub>x</sub>I<sub>3</sub>/PTA/V<sub>2</sub>O<sub>5-δ</sub>/Al) based on MAPb<sub>1-x</sub>Eu<sub>x</sub>I<sub>3</sub> (a) and Cs<sub>0.12</sub>FA<sub>0.88</sub>Pb<sub>1-x</sub>Eu<sub>x</sub>I<sub>3</sub> (b), where  $x = 0.001, 0.005$ , and  $0.01$ .

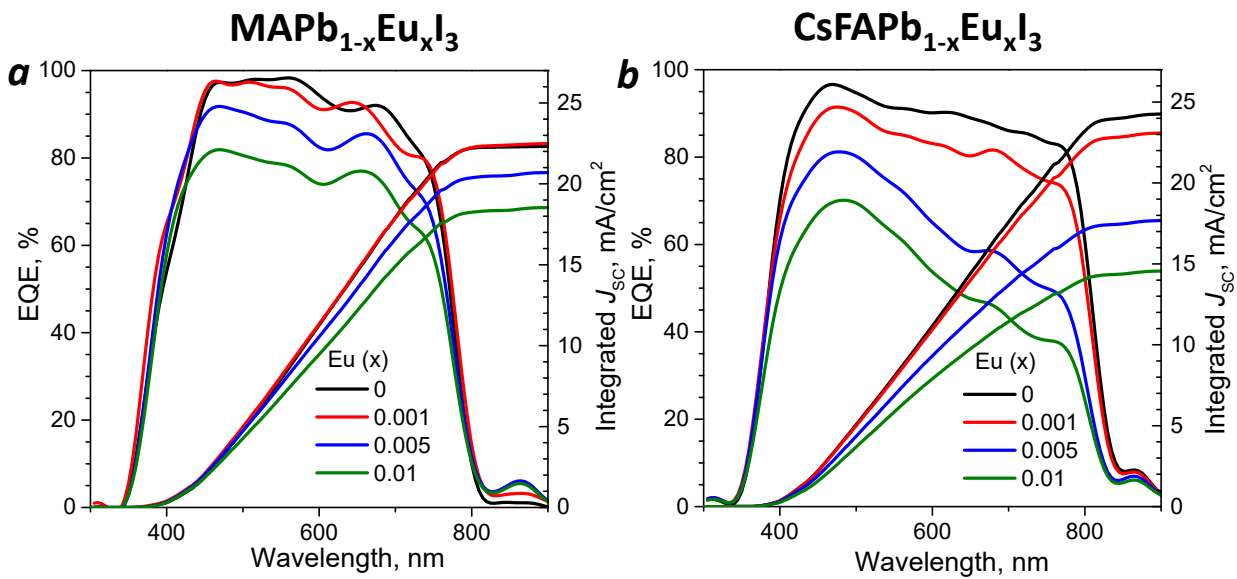


Figure S7. The EQE spectra of the solar cells with the structure of ITO/SnO<sub>2</sub>/PCBA/perovskite/PTA/V<sub>2</sub>O<sub>5-δ</sub>/Al based on the or MAPb<sub>1-x</sub>M<sub>x</sub>I<sub>3</sub> (a) and Cs<sub>0.12</sub>FA<sub>0.88</sub>Pb<sub>1-x</sub>Eu<sub>x</sub>I<sub>3</sub> (b), where x= 0, 0.001, 0.05, and 0.01.

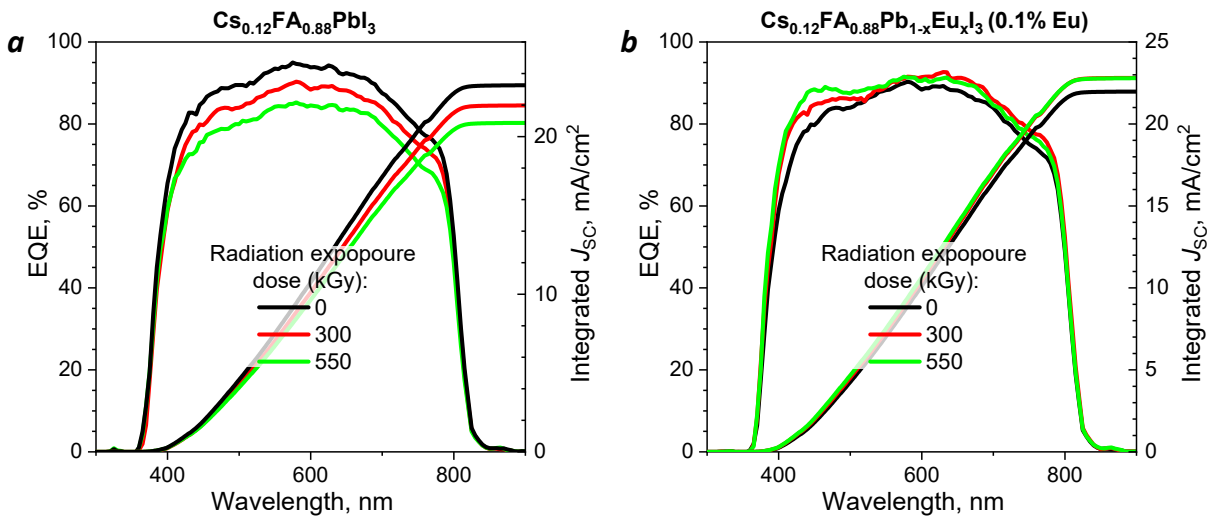


Figure S8. Evolution of the EQE spectra of the PET/ITO/PTA/Perovskite/PCBM/BCP/Al solar cells upon exposure to <sup>60</sup>Co gamma rays.

Table S1. Surface composition of the  $\text{MAPb}_{1-x}\text{Eu}_x\text{I}_3$  perovskite films (in at.%).

<b>Sample</b>	<b>Si</b>	<b>C</b>	<b>O</b>	<b>N</b>	<b>N:(Pb+Eu)</b>	<b>Pb</b>	<b>I</b>	<b>I:(Pb+Eu)</b>	<b>Eu</b>	<b>Eu:Pb</b>
undoped	5.6	45.9	9.2	6.6	0.67	9.8	22.9	2.33	-	-
1% Eu	6.1	44.3	14.2	5	0.48	9.3	20.1	1.95	1.0	0.11
5% Eu	4.4	54.0	13.3	3.9	0.36	6.2	16.1	1.93	2.1	0.34
10% Eu	3.0	53.7	13.7	4.5	0.49	5.1	16.0	1.76	4.0	0.78

Table S2. Surface composition of the  $\text{Cs}_{0.12}\text{FA}_{0.88}\text{Pb}_{1-x}\text{Eu}_x\text{I}_3$  perovskite films (in at.%).

<b>Sample</b>	<b>C</b>	<b>O</b>	<b>N</b>	<b>N:(Pb+Eu)</b>	<b>Pb</b>	<b>I</b>	<b>Cs</b>	<b>I:(Pb+Eu)</b>	<b>Eu</b>	<b>Eu:Pb</b>
undoped	30	2.1	20.1	1,53	13.1	33.4	1.3	2.55	-	-
1% Eu	42.2	5.7	14.7	1,37	9	25.8	0.9	2.41	1.7	0.19
5% Eu	43.3	13.5	8.8	0,80	5.5	22.8	0.6	2.07	5.5	1
10% Eu	47.7	16.7	6	0,55	5.5	18	0.7	1.81	5.4	0.98
20% Eu	46.2	20.6	5.2	0,53	3.5	17.5	0.6	1.77	6.4	1.83

Table S3. The average and the best (in brackets) values of power conversion efficiency ( $\eta$ ), open-circuit voltage ( $V_{OC}$ ), short-circuit current density ( $J_{SC}$ ), and fill factor ( $FF$ ) of the ITO/SnO<sub>2</sub>/PCBA/MAPb<sub>1-x</sub>M<sub>x</sub>I<sub>3</sub> or Cs<sub>0.12</sub>FA<sub>0.88</sub>Pb<sub>1-x</sub>Eu<sub>x</sub>I<sub>3</sub>/PTA/V<sub>2</sub>O<sub>5- $\delta$</sub> /Al devices (x = 0.001, 0.005 and 0.01).\*

Composition	Scan	V <sub>OC</sub> , V	J <sub>SC</sub> , mA cm <sup>-2</sup>	FF, %	PCE, %
<b>MAPb<sub>1-x</sub>Eu<sub>x</sub>I<sub>3</sub></b>					
<b>x = 0 (Pristine)</b>	Forward	(1.042) 1.029±0.009	(23.3) 23.1±0.1	(74.5) 72.0±3.1	(17.6) 17.1±0.8
	Reverse	(1.043) 1.029±0.009	(23.3) 23.0±0.2	(75.1) 73.6±2.1	(17.9) 17.5±0.6
<b>x = 0.001</b>	Forward	(1.047) <b>1.041±0.004</b>	(23.5) <b>23.3±0.3</b>	(74.4) <b>73.3±0.8</b>	(17.9) <b>17.7±0.2</b>
	Reverse	(1.047) <b>1.041±0.005</b>	(23.4) <b>23.2±0.3</b>	(75.2) <b>75.0±0.6</b>	(18.2) <b>18.1±0.2</b>
<b>x = 0.005</b>	Forward	(1.034) 1.024±0.008	(23.0) 22.9±0.1	(69.2) 65.7±2.3	(16.3) 15.4±0.5
	Reverse	(1.035) 1.021±0.009	(23.1) 23.0±0.1	(68.0) 63.9±2.8	(16.0) 15.0±0.7
<b>x = 0.01</b>	Forward	(0.987) 0.982±0.005	(20.4) 20.0±0.3	(50.2) 49.0±0.9	(9.7) 9.6±0.1
	Reverse	(0.986) 0.976±0.008	(20.2) 19.9±0.3	(52.0) 50.8±1.2	(10.1) 9.8±0.2
<b>Cs<sub>0.12</sub>FA<sub>0.88</sub>Pb<sub>1-x</sub>Eu<sub>x</sub>I<sub>3</sub></b>					
<b>x = 0 (Pristine)</b>	Forward	(0.905) 0.904±0.004	(24.9) 23.6±0.7	(72.7) 71.8±0.7	(16.3) 15.3±0.5
	Reverse	(0.925) 0.908±0.007	(25.2) 24.0±0.9	(74.4) 71.8±1.7	(16.8) 15.7±0.9
<b>x = 0.001</b>	Forward	(0.911) <b>0.908±0.003</b>	(24.6) <b>24.5±0.1</b>	(70.4) <b>70.0±1.1</b>	(15.6) <b>15.5±0.1</b>
	Reverse	(0.925) <b>0.922±0.003</b>	(24.5) <b>24.4±0.1</b>	(71.8) <b>71.5±0.4</b>	(16.2) <b>16.1±0.1</b>
<b>x = 0.005</b>	Forward	(0.877) 0.813±0.031	(23.8) 23.3±0.5	(64.4) 58.7±2.8	(12.6) 11.1±0.7
	Reverse	(0.873) 0.816±0.029	(23.7) 23.2±0.5	(65.0) 61.3±2.0	(12.7) 11.6±0.6
<b>x = 0.01</b>	Forward	(0.749) 0.740±0.008	(10.3) 10.0±0.4	(52.3) 51.6±0.9	(4.0) 3.8±0.3
	Reverse	(0.743) 0.735±0.009	(10.9) 10.4±0.4	(49.3) 48.5±0.9	(4.0) 3.7±0.3

\* - The J-V curves were measured in forward and reverse directions with the scan rate of 0.01 V/s

Table S4. The average and the best (in brackets) values of power conversion efficiency ( $\eta$ ), open-circuit voltage ( $V_{OC}$ ), short-circuit current density ( $J_{SC}$ ), and fill factor (FF) of the PET/ITO/PTA/Cs<sub>0.12</sub>FA<sub>0.88</sub>Pb<sub>1-x</sub>Eu<sub>x</sub>I<sub>3</sub> (x=0 and 0.001)/PCBM/BCP/Al devices.\*

<b>Composition</b>	<b>Scan direction</b>	<b>V<sub>OC</sub>, V</b>	<b>J<sub>SC</sub>, mA cm<sup>-2</sup></b>	<b>FF, %</b>	<b>PCE, %</b>
<b>x = 0.001</b>	Forward	(0.958) 0.950±0.022	(22.6) 22.0±0.5	(79.3) 73.7±4.3	(17.1) 15.4±1.2
	Reverse	(0.983) 0.949±0.023	(22.5) 21.8±0.8	(78.7) 75.4±2.1	(17.5) 15.6±1.3
<b>x = 0 (Pristine)</b>	Forward	(1.022) 0.982±0.059	(23.0) 22.4±1.1	(78.2) 71.3±7.5	(18.4) 15.7±1.8
	Reverse	(1.026) 0.978±0.060	(23.2) 22.4±1.0	(79.0) 72.5±7.3	(19.0) 15.9±2.2

\* - The J-V curves were measured in forward and reverse directions with the scan rate of 0.01 V/s